

Article

Substrate-Integrated Waveguide PCB Leaky-Wave Antenna Design Providing Multiple Steerable Beams in the V-Band

Matthias Steeg¹ , Naruto Yonemoto², Jonas Tebart¹ and Andreas Stöhr^{1,*}

¹ ZHO/Optoelectronics, University of Duisburg-Essen, 47057 Duisburg, Germany; matthias.steeg@uni-due.de (M.S.); jonas.tebart@stud.uni-due.de (J.T.)

² Electronic Navigation Research Institute, National Institute of Maritime, Port and Aviation Technology, Chofu, Tokyo 1820012, Japan; yonemoto@mpat.go.jp

* Correspondence: andreas.stoehr@uni-due.de; Tel.: +49-203-379-2825

Received: 23 October 2017; Accepted: 4 December 2017; Published: 7 December 2017

Abstract: A periodic leaky-wave antenna (LWA) design based on low loss substrate-integrated waveguide (SIW) technology with inset half-wave microstrip antennas is presented. The developed LWA operates in the V-band between 50 and 70 GHz and has been fabricated using standard printed circuit board (PCB) technology. The presented LWA is highly functional and very compact supporting 1D beam steering and multibeam operation with only a single radio frequency (RF) feeding port. Within the operational 50–70 GHz bandwidth, the LWA scans through broadside, providing over 40° H-plane beam steering. When operated within the 57–66 GHz band, the maximum steering angle is 18.2°. The maximum gain of the fabricated LWAs is 15.4 dBi with only a small gain variation of +/−1.5 dB across the operational bandwidth. The beam steering and multibeam capability of the fabricated LWA is further utilized to support mobile users in a 60 GHz hot-spot. For a single user, a maximum wireless on-off keying (OOK) data rate of 2.5 Gbit/s is demonstrated. Multibeam operation is achieved using the LWA in combination with multiple dense wavelength division multiplexing (WDM) channels and remote optical heterodyning. Experimentally, multibeam operation supporting three users within a 57–66 GHz hot-spot with a total wireless cell capacity of 3 Gbit/s is achieved.

Keywords: 5G mobile communications; beam steering; fiber-wireless communication; leaky-wave antennas; millimeter wave wireless; radio-over-fiber; substrate-integrated waveguide

1. Introduction

The large available bandwidth at mm-wave frequencies especially in the 60 GHz band enables new use case scenarios such as the 5G hot-spot proposed for the next generation of mobile communications (5G) [1–4]. Generally, 5G is expected to bring a revolution to mobile communications: a 1000-fold increase in mobile data traffic and a substantially larger number of connected users per cell [5]. This is to be achieved by using a wider RF bandwidth and greater spectral efficiency as cell size is decreased [1–3]. These requirements can be met using carrier frequencies in the 57–66 GHz band where a large bandwidth is internationally available. To mitigate the higher free-space path loss in the millimeter-wave range, directive antennas are considered [2–4,6]. However, the usage of directive antennas requires beam steering to enable user mobility and multiple independent beams so that multiple users can be supported in dense user scenarios simultaneously. Therefore, steerable directive antennas are a key technology for supporting multiple users in dense user scenarios [3,6,7]. Another key technology is optical fiber for fronthauling the high capacity 5G hot-spots and small cells [3,8]. Radio-over-fiber (RoF) is used as the transport technology between the baseband unit and the antenna for reducing implementation cost and latency through direct optical-to-electrical (O/E)

conversion [8]. Thereby, digital-to-analogue conversion and complex signal processing can be avoided. Further benefits of RoF include that it allows for centralizing network functions, which is expected to save cost, especially when a high number of radio access units (RAUs) is considered [3,8].

The application of millimeter-waves for wireless access is investigated intensely with the advent of 5G [2,3] and has already led to prototype devices for 28 GHz phased array beam steering, which are widely discussed and referenced [6]. Despite the technological challenges at higher frequencies, e.g., the 60 GHz band, active phased array beam steering solutions have been reported [7,9]. However, because scaling issues have led to more input ports, greater complexity, and more power consumption, these solutions only support the steering of one beam and a limited baseband signal bandwidth [3,6,7]. Thus, they can only support multiple users within one beam and only use frequency or time division multiple access [7], which limits user experience. Due to these constraints, passive solutions such as lens assisted beam switching or Butler matrix implementations have also been considered [3,10]. While these passive solutions can provide higher signal bandwidth and do not increase power consumption, they still require multiple signal inputs to allow multiple beam operation. Thus, their multi-user support scales poorly, as it requires additional fronthaul capacity and increases the size of the antenna integration. Thus, passive low-cost, multiple-beam solutions, which support a large overall bandwidth, still need to be systematically addressed.

For the sake of completeness, it should be noted that the 5G mobile terminals will likely employ different antenna types, as there the vital requirement is to cover all internationally available bands with a very limited form-factor. This emphasizes multi-band operation and wideband coverage in contrast to high gain and beam steering capabilities in base stations. Thus, likely candidates for 5G mobile terminals are printed monopoles for sub 6 GHz 5G and small integrated antenna-on-chip MIMO configurations for mm-wave 5G [11,12].

In this paper, a compact and low-cost substrate-integrated waveguide (SIW) leaky-wave antenna (LWA) for 60 GHz band operation is proposed, and it was used to support multiple users in a 60 GHz hot-spot is proposed. In an LWA, beam steering was achieved by changing the radio frequency (RF) [13–16]. The fabricated LWA provides 1D H-plane beam steering as well as multibeam operation with 20 GHz operational bandwidth. Since only one RF port is required for multibeam operation, the proposed LWA can be made compact compared to multiple-input-multiple-output (MIMO) or phased array antenna solutions. This makes the LWA an ideal candidate for 5G hot-spots, which are proposed by the ITU-R as part of the enhanced mobile broadband (eMBB) family of 5G, where high user densities are foreseen [1,4]. Furthermore, installations with a large number of small 5G cells with high spectrum reuse synergize with the proposed low-cost PCB LWA.

In this context, the developed LWA supports network function centralization, as beam steering is achieved via optical frequency scanning. This approach does not require additional control signals. In addition, by using dense wavelength division multiplexing (DWDM) optical channels in the RoF feeding network and remote optical heterodyning, multiple steerable beams are generated by the LWA. This allows supporting multiple mobile users in a hot-spot with individual beams carrying individual user data.

The paper is organized as follows: First, the 60 GHz substrate integrated waveguide leaky-wave antenna design is outlined and its fundamental properties explained. The in-depth antenna characterization of the SIW LWA is then presented, beginning with the measurement setup and showing its performance based on scattering parameters, gain, radiation patterns, beam steering behavior, and polarization. After that, the application of the SIW LWA for providing beam steering capabilities to centralized 5G hot-spots based on fiber-wireless RoF transport is described. Finally, single link and point-to-multipoint fiber-wireless transmission experiments are demonstrated using the SIW LWA.

2. Substrate-Integrated Waveguide Leaky-Wave Antenna Design

The proposed periodic leaky-wave antenna design based on a substrate-integrated waveguide consists of a repetition of 12 unit cells. The design was conceived employing the 3D full wave

electromagnetic simulation tool HFSS (High Frequency Structure Simulator; Ansys, Canonsburg, PA, USA), which is based on the finite element method (FEM). The chosen PCB material was Rogers RT/duroid 5880 (Rogers Corporation, Chandler, AZ, USA) because of its low dissipation factor of 0.0009 at 10 GHz. In order to reduce dielectric losses, a thin laminate with a thickness of 0.254 mm was used, which also represents the height of the SIW [17]. The SIW is designed for a lower cutoff frequency of 40 GHz to allow single mode operation up to 80 GHz with a linear dispersion slope in the frequency range of interest between 50 and 70 GHz [16,18]. Based on the permittivity of the employed laminate of 2.2, this results in a width W of 2.6 mm between the via post walls. The via holes have a 0.15 mm diameter and are arrayed with a pitch P of 0.3 mm. In each unit cell, a 180 μm wide longitudinal microstrip line is inset in the SIW, as depicted in Figure 1. The microstrip lines act as the radiating elements. Their length $L = 1.67$ mm corresponds to the guided wavelength at 61.3 GHz, which is the designed broadside frequency in the center of the 57–66 GHz band. The rectangular slots forming the microstrip lines extend up to the via post walls. The utilization of longitudinal microstrips inset in the SIW is a complementary approach to transversal slot SIW LWAs, which have already been shown, e.g., in [14]. This SIW LWA approach allows for the manipulation of the symmetry of the unit cell, which is a fundamental property for LWAs, in the longitudinal as well as the transversal axis [15]. Here, the microstrip lines are off-centered by 40 μm in the x -direction, as can be seen in the inset of Figure 1. Due to this asymmetry, the open-stopband is decreased and broadside radiation is increased [15].

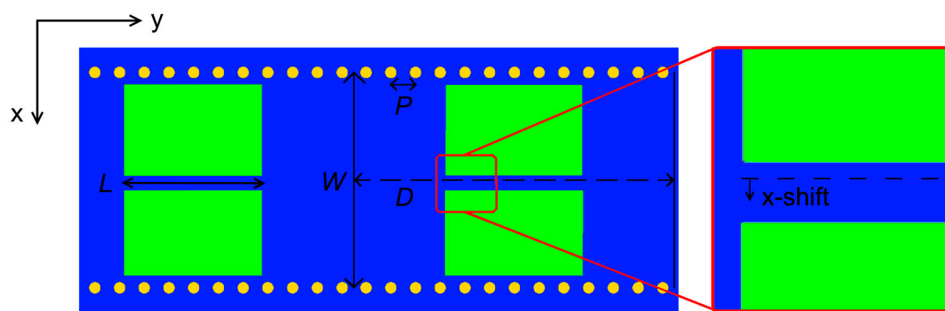


Figure 1. Top view of the proposed periodic substrate-integrated waveguide (SIW) leaky-wave antenna (LWA) design based on a printed circuit board (PCB) with top metallization (blue) and dielectric (green), where W denotes the 2.6 mm width of the SIW, P the 0.3 mm pitch of the via holes (yellow) with 0.15 mm diameter and D the 3.9 mm periodicity of the array.

For investigating the operational bandwidth and the beam steering behavior of the SIW LWA, Eigenmode simulations were carried out to study the natural resonances of the examined structure. When applied to the SIW LWA unit cell, Eigenmode simulations reveal the waveguide modes with their corresponding Eigenfrequencies [19]. To take into account that, in the LWA, the wave propagates through consecutive unit cells, periodic boundaries are defined at both ends of the unit cell. This allows to enforce a phase difference between the unit cells, which basically relates to the phase taper of an antenna array. The normalized phase difference between two consecutive unit cells is shown in the dispersion diagram in Figure 2. It can be observed, that the Eigenfrequencies change based on the enforced phase difference. Thus, at different frequencies, the phase difference between the radiating elements and consequently the beam angle changes and frequency based beam steering is obtained. In this regard, periodic LWAs have the property to radiate in the left-handed (LH) region, where β is negative, and in the right-handed (RH) region, where β is positive. Thus, for decreasing frequencies in the LH region, the beam is steered towards backfire, and for increasing frequencies in the RH region towards endfire [13]. At the transit from the LH to the RH region, broadside radiation is obtained, which is at 61.3 GHz for this design. The frequency difference between the LH and RH mode at 0° phase difference is the open-stopband, which generally causes degraded radiation at broadside [13].

In this SIW LWA design, a very narrow open-stopband of less than 23 MHz is achieved thanks to the unit cell asymmetry. Furthermore, the design exhibits an almost linear dispersion slope with a similar gradient for the LH and RH regions up to a phase difference of $\pi/2$. Thus, within the operational bandwidth from 50 to 70 GHz, an almost linear relation between beam angle and radiation frequency is projected, when considering the beam steering behavior of LWAs [13]:

$$\sin \theta \approx \beta_{-1}/k_0 = \lambda_0/\lambda_g - \lambda_0/D. \quad (1)$$

In Equation (1), the dependence of the radiated beam angle θ on the vacuum wave number k_0 and the phase coefficient β_{-1} of the TE mode in the LWA is given. As denoted by the index, the modes radiated by periodic LWAs are of the $n = -1$ space harmonic. The right side of the equation gives the beam steering behavior based on the vacuum wavelength λ_0 , the guided wavelength λ_g and the periodicity D . Since the sine function can be well approximated as linear for low angles, a linear gradient of β_{-1} will consequently yield approximately linear beam steering. In the next section, we want to verify the estimations on the SIW LWA beam steering behavior through antenna characterization and further provide the simulated and measured gain of the complete 12 unit cell periodic leaky-wave antenna.

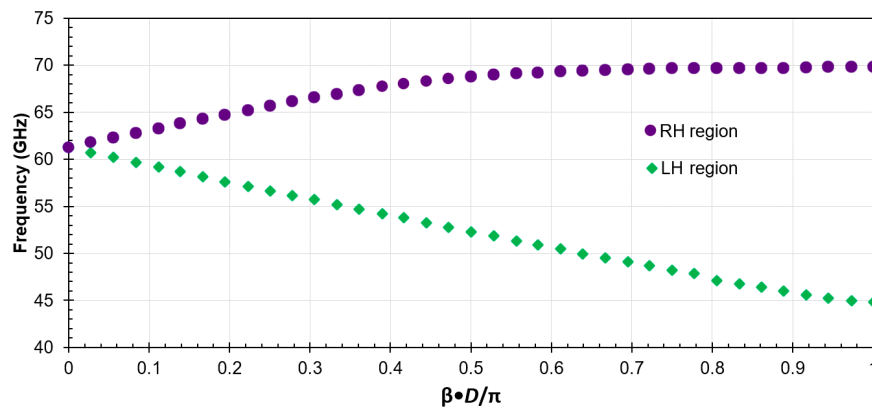


Figure 2. Dispersion diagram of the unit cell of the LWA based on Eigenmode simulations. The frequencies of the Eigenmodes are plotted versus the normalized phase change for the right-handed (RH) region (circles, purple) and the left-handed (LH) region (diamonds, green).

3. Antenna Characterization

3.1. Antenna Measurement Setup

The antenna characterization was conducted in an anechoic chamber equipped for millimeter-wave measurements up to 110 GHz. The measurement system consists of two signal generators and a microwave receiver as shown in Figure 3. A frequency multiplier connected to the signal generator transmits the test signal in the frequency range from 50 to 75 GHz. The LWA is connected to the transmitter. After 4 m of wireless transmission, a horn antenna connected to a harmonic mixer receives the test signal emitted by the LWA. The gain of the LWA (here: antenna under test (AUT)) is calculated through the difference in path loss to a calibrated horn antenna with known gain. Thereby, the frequency response of the measurement system and especially of the external multiplier is cancelled out.

For the measurements, the antenna assembly depicted in Figure 4 was utilized, which shows the fabricated PCB contacted by coaxial end launch connectors (ELCs), which are presented in [20]. The ELCs also screw the PCB to brass brackets, which provide mechanical fixtures. A coupled line (CL) transition is used between the SIW LWA and the grounded coplanar waveguide (GCPW), which is interfaced by the ELC. The CL transition further performs impedance matching between the

waveguides and prevents a DC short for the GCPW interface, allowing for integration of photodiodes and/or amplifiers. Since the SIW LWA is symmetric in its longitudinal axis, its two ELC ports inherit the same radiation characteristics, albeit mirrored. In the setup, one port is utilized for feeding the signal, and the other is terminated by a matched load to avoid back reflections.

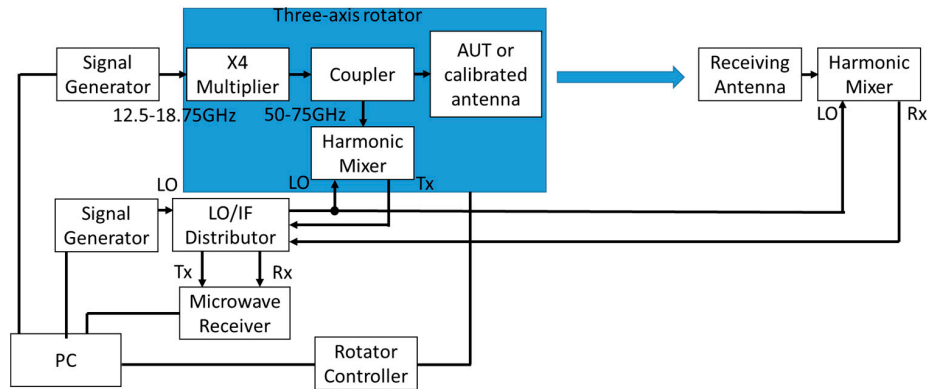


Figure 3. Schematic diagram of the antenna measurement setup.

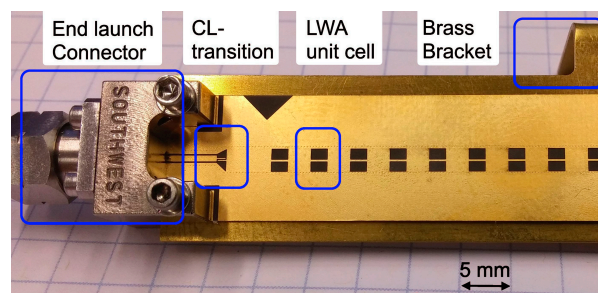


Figure 4. Photograph of the antenna assembly consisting of the fabricated SIW LWA PCB with coupled-line (CL) transition, brass bracket and coaxial end launch connector (ELC).

For evaluating the losses of the SIW LWA, a vector network analyzer (VNA) was employed to measure the 2-port scattering parameters. Thru-Reflect-Line (TRL) test structures were measured in advance to de-embed the connector and adapter losses and evaluate waveguide losses.

3.2. Antenna Scattering Parameters and Gain

Because of the longitudinal symmetry, the matrix of the 2-port scattering parameters is expected to be bisymmetric, meaning that $S_{11} = S_{22}$ and $S_{12} = S_{21}$. Therefore, Figure 5 only shows the simulated and measured scattering parameters S_{11} and S_{21} . For S_{21} , a very good agreement between simulated and de-embedded measured scattering parameters was observed. Here, waveguide losses of on average 0.658 dB/cm were de-embedded from S_{21} . These losses were experimentally determined using the TRL test structures with different lengths. A substantial difference from the low simulated SIW losses around 0.2 dB/cm [17], which are based on the data sheet values, was observed. However, it has been shown that the data sheet values, which are determined for 10 GHz, significantly underestimate the dissipation factor of the used laminate at 60 GHz [21]. This results in measured transmission line losses, which are larger than expected from the simulations. For example, for a similar laminate in [20], a microstrip line loss of about 1 dB/cm at 50 GHz was experimentally determined. For S_{11} , some deviations were observed, which can at least in part be attributed to the screw-on ELCs. During the measurements, it was observed that the precise screwing of the ELCs affect the position and height of the reflection peaks. Notably the fabricated SIW LWA achieved a low S_{11} around broadside, where resonant matching of the radiating elements and CL transition is designed.

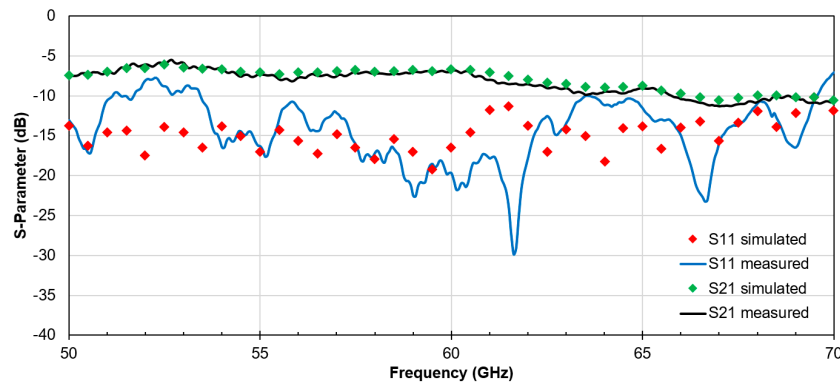


Figure 5. Scattering parameters of the SIW LWA in dB over the frequency range from 50 to 70 GHz. The simulated values of S_{11} (red, diamonds) and S_{21} (green, diamonds) are shown together with the de-embedded measured values of S_{11} (blue, solid line) and S_{21} (black, solid line).

In Figure 6, the simulated and measured spectral antenna gain is depicted between 50 and 67 GHz. As can be seen, the SIW LWA shows a maximum gain of 15.4 dBi at 62 GHz. The gain is relatively flat over the frequency range with a variation of only ± 1.5 dB from the mean gain of 14.0 dBi. The measured values show no major gain degradation at broadside frequency which is traced back to unit cell asymmetry.

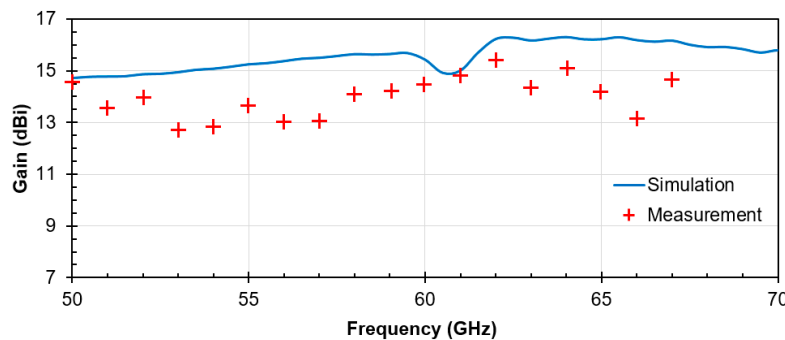


Figure 6. Simulated (solid line, blue) and de-embedded measured gain (crosses, red) of the presented LWA in dBi plotted over the radio frequency.

3.3. Radiation Pattern and Beam Steering

The simulated and measured H-plane radiation patterns of the SIW LWA between beam angles from -45° to $+45^\circ$ are shown in Figure 7. In general, a good agreement between the simulated and measured spectral gain is observed. There is only a small and almost constant shift between the simulated and measured beam angle of about 1° . This is traced back to minor inaccuracies in mounting the SIW LWA assembly to the measurement system. From Figure 7, one can furthermore observe that the maximum gain for 57 GHz and 66 GHz is at beam angles of -9.8° and $+8.4^\circ$, respectively. Thus, 1D beam steering of 18.2° was achieved when the RF was tuned within the frequency range of interest, from 57 to 66 GHz. The side lobe suppression was 14 dB at 50 GHz RF and changed towards lower values for increased radio frequencies, always staying above 11 dB. The 3-dB beam width of the LWA in the H-plane lay between $\theta_{3dB,H} = 6.8^\circ$ at 50 GHz and $\theta_{3dB,H} = 5.2^\circ$ at 66 GHz. This means that, when the gain of the antenna is flat, the directivity slightly increases with frequency. This increase in directivity is offset by higher losses at higher frequencies, which can be deduced from the decreasing S_{21} .

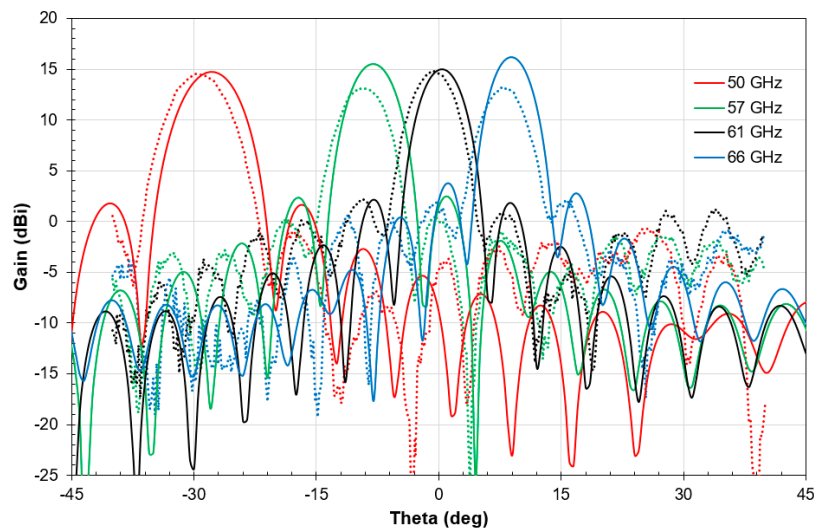


Figure 7. H-plane radiation patterns as the measured (dots) and simulated (solid lines) gain of the SIW LWA over the beam angle theta in degrees at frequencies of 50 GHz (red), 57 GHz (green), 61 GHz (black), and 66 GHz (blue).

Figure 7 also gives a first impression on the multibeam capabilities of the SIW LWA. Thereby, multibeam operation can be achieved by simply using multiple RF carrier frequencies, which are radiated at different beam angles according to their radiation patterns. Experimental results for multibeam data transmission are presented in the next section.

Next, the beam steering behavior was analyzed. In Figure 8, the beam angle is plotted versus the frequency of operation. Again, a very good agreement between Eigenmode simulations, far-field simulations, and antenna measurements was observed. Overall, 40° beam steering was obtained for the entire 50–70 GHz frequency range, confirming the simulations of the design [16]. Furthermore, almost linear beam steering with a coefficient of approximately $\delta\theta/\delta f = 2.25^\circ/\text{GHz}$ was achieved thanks to the almost linear dispersion slope shown in Figure 2. Together with the measured 3-dB beam widths, the resulting coherence bandwidths can easily be estimated based on the following equation and lie in the range from $\delta f_{\text{coh},50} = 3.0$ GHz at 50 GHz to $\delta f_{\text{coh},66} = 2.3$ GHz at 66 GHz.

$$\delta f_{\text{coh}} = \theta_{3\text{dB}} / (\delta\theta / \delta f). \tag{2}$$

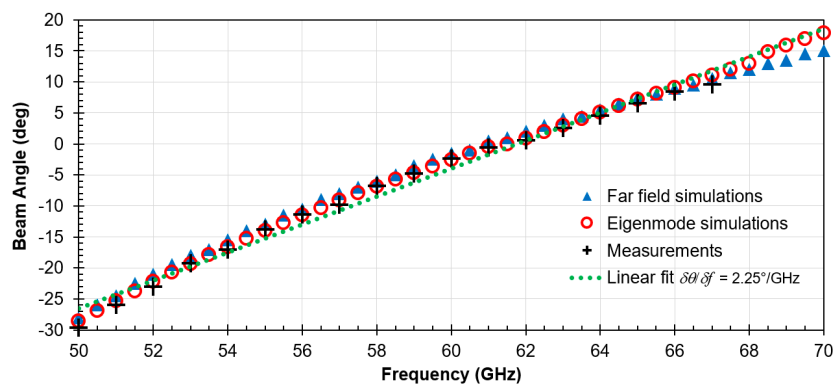


Figure 8. H Beam steering behavior of the SIW LWA as beam angle over frequency from far field simulations (triangles, blue), Eigenmode simulations (circles, red), measurement results (crosses, black), and their linear fit (green).

3.4. Antenna Polarization and Efficiency

Since the fundamental radiating element of the proposed SIW LWA is a linearly polarized microstrip, one can also expect the SIW LWA to be linearly polarized. This was experimentally confirmed from the measured H-plane cross polarization discrimination (XPD), which is 24.83 dB. The measured normalized radiation patterns of the E-plane for co-polarization and cross-polarization at 60 GHz are shown in Figure 9. As to be expected, the E-plane did not provide a high directivity, as there were no arrayed radiating elements in this plane. The measured E-plane 3-dB beam width is $\varphi_{3\text{dB}} = 75^\circ$. The radiation efficiency η_{rad} can be calculated as the quotient of gain g and directivity d . Therefore, by calculating the directivity from the 3-dB beam widths of the E-plane and H-plane radiation patterns, using Equation (3), the radiation efficiency can be estimated [22]. This results in an estimated broadside radiation efficiency of 39.2% at 61 GHz and a maximum efficiency of 45.0% at 50 GHz.

$$\eta_{\text{rad}} = g/d \approx g/(32,400/\theta_{3\text{dB}}/\varphi_{3\text{dB}}). \quad (3)$$

In Figure 9, it can be further observed that the cross-polarization is higher than the co-polarization for beam angles lower than -45° and larger than 55° . This causes a reduced XPD in the E-plane of only 5.66 dB. A potential approach to increase directivity and XPD in the E-plane could be to use multiple SIW LWA arrays and feed them from the same input employing a substrate-integrated power divider.

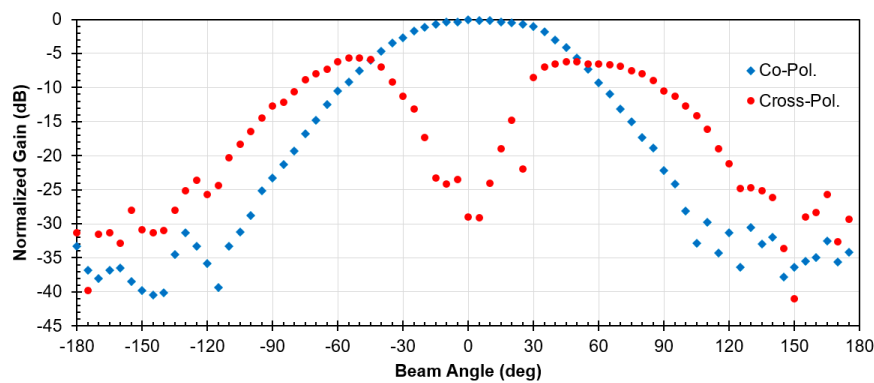


Figure 9. E-plane radiation pattern of the presented SIW LWA at 60 GHz radio frequency as the normalized gain in dB over beam angle in degrees for the co-polarization (diamonds, blue), and cross-polarization (circles, red).

4. Application of the SIW LWA for Radio-Over-Fiber-Based 5G Hot-Spots

4.1. Radio-Over-Fiber Photonic Beam Steering via SIW Leaky-Wave Antennas

In this section, we seek to outline the application of the presented SIW LWA for providing beam steering functionality for 5G hot-spots. Therefore, the architecture of the targeted communication system including fiber-based and wireless links is illustrated in Figure 10. This system is comprised of three parts: the central baseband unit (CBU), the radio access unit (RAU), and the mobile unit(s). At the CBU, an optical carrier from a signal laser is modulated with data. After amplification and several km SMF, the signal arrives at the RAU, where a local oscillator laser (LD LO) is added and a high frequency photodiode (HF PD) generates the RF signal as the beat frequency of the two lightwaves via heterodyne detection. After amplification, the RF signal is radiated to the mobile unit(s). There it is received, amplified again, and downconverted to baseband via a Schottky barrier diode detector (SBD). Since the SBD acts as an envelope detector, the mobile unit does not require a LO, and a large operational bandwidth is obtained without tuning any components at the receiver. The fronthaul link between CBU and RAU is essentially a radio-over-fiber scheme with optical upconversion, which allows the radio frequency to be changed by tuning the wavelength of either the local oscillator

laser or the signal laser. Thus, by employing the SIW LWA, the beam angle of the transmitting antenna can be steered by tuning the signal or local lasers and thus changing the RF. This means that centralized beam steering is possible, enabling user mobility, and no additional control signals are necessary. Furthermore, by generating multiple densely spaced optical carrier at the CBU, multiple mobile users can be served by this DWDM scheme. The data for every user can thus be modulated onto a separate optical carrier, which can be tuned independently to provide beam steering of the individual beams. To multiplex the individual channels for each user onto one fiber, only simple passive combiners are required. At the RAU, no demultiplexing is required as the individual optical channels are inherently radiated in different directions towards the mobile users. This way, wavelength multiplexing is inherently converted to spatial multiplexing.

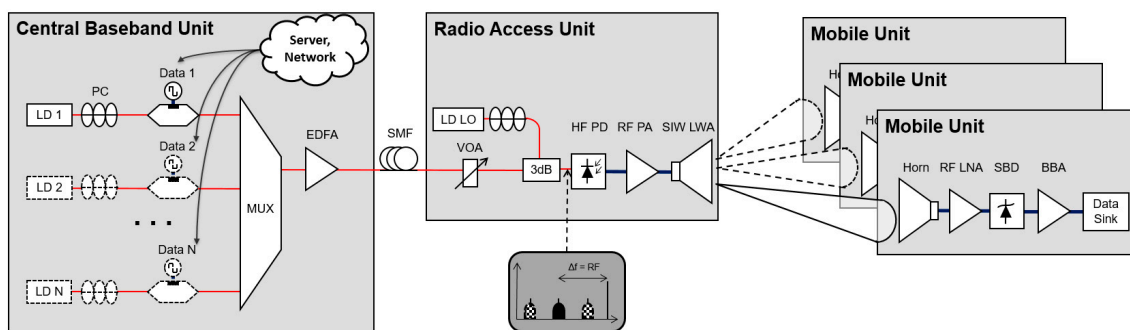


Figure 10. Proposed radio-over-fiber (RoF) based architecture for serving multiple mobile users via an optical dense WDM scheme and the presented SIW leaky-wave antenna.

4.2. Radio-Over-Fiber Point-To-(Multi)Point Data Transmission Experiments

The fabricated SIW LWA was utilized for fiber-wireless data transmission experiments in the V-band with the described setup. The employed commercial telecom laser diodes are integrable tunable laser assemblies (ITLAs; Pure Photonics PPLC200, San Jose, CA, USA), which can be tuned flexibly across the whole C-band (191.5–196.25 THz). They are external cavity lasers with a low linewidth <math><100\text{ kHz}</math>, which use additional Etalon filters to obtain monomode operation. Since they already contain a thermo-electric cooler (TEC) and a laser diode driver to adjust their output power from 7 to 15.5 dBm, they allow compact packaging. The lasers are controlled via an RS-232 serial interface. Here, an optical carrier at $\lambda = 1550\text{ nm}$ is externally OOK modulated by employing a Mach-Zehnder modulator (MZM; Fujitsu, Tokyo, Japan) and a pulse pattern generator, which generates a pseudorandom binary sequence (PRBS) with a word length of $2^{31}-1$. The optical baseband signal is amplified by an Erbium-doped fiber amplifier (EDFA; Calmar Laser, Pablo Alto, CA, USA) to +10 dBm and transmitted over 10 km single mode fiber (SMF) to a remote photodiode with a 70 GHz bandwidth and a V-type interface (Finisar, Sunnyvale, CA, USA). The generated RF signal is then amplified by an amplifier with 30 dB gain up to a maximum power of +18 dBm and fed to the SIW LWA. An optical LO is added to generate the 61 GHz RF carrier by optical heterodyning. A 23 dBi horn antenna receives the signal at the mobile unit after a 2 m wireless distance. An LNA with a 35 dB gain and a 4.5 dB noise figure is employed before the V-band SBD with a responsivity of 2000 V/W. After downconversion and amplification of the baseband signal, an error detector is utilized to evaluate the received signal quality by its bit error rate (BER). A variable optical attenuator (VOA; Anritsu, Atsugi, Japan) is employed at the RAU to decrease the optical signal power and consequently the RF power to yield different signal-to-noise ratios for BER measurements.

The OOK data rate was modified from 0.5 to 2.5 Gbit/s in 0.5 Gbit/s steps, and the measured BERs with respect to received RF power are shown in Figure 11. As can be seen, error-free ($\text{BER} < 10^{-9}$) transmission was achieved up to 2.0 Gbit/s. For 2.5 Gbit/s, forward-error correction (FEC) would have been required. This was traced back to the coherence bandwidth of the SIW LWA. Based on the

rise and fall times of the measured eye diagrams (see inset in Figure 11), the bandwidth of the detected signals was determined to be 1.3 GHz. Considering that the transmission bandwidth is twice as large for OOK, this corresponds well to the determined coherence bandwidth of the antenna.

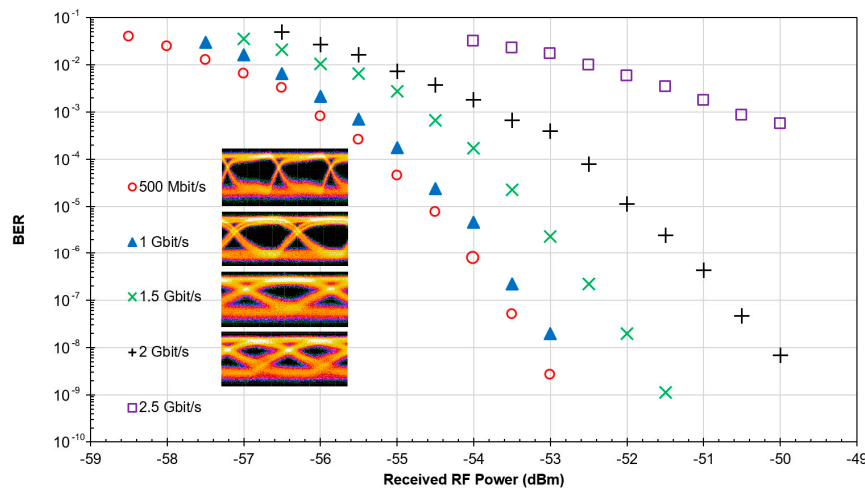


Figure 11. Measured bit error rate (BER) over received radio frequency (RF) power at on-off keying (OOK) data rates from 500 Mbit/s to 2.5 Gbit/s. Insets show the quasi error free eye diagrams.

Of course, data rates can be increased using complex modulation formats, as reported in [22], where 6 Gbit/s was achieved for a single beam using the same SIW LWA and 64-QAM-OFDM modulation (quadrature amplitude modulation with orthogonal frequency-division multiplexing). However, even for simple OOK modulation, the presented SIW LWA supports multiple Gbit/s transmission rates, which is essential for 5G communications.

The large overall bandwidth of the SIW LWA can be exploited in synergy with its 1D beam steering capabilities to support multiple users simultaneously. To demonstrate this, three 1 Gbit/s OOK optical baseband channels with a ultra-dense channel spacing of 3 GHz were generated at the CBU. To enable comparable results, identical lasers and MZMs were used to enable comparable results. The optical baseband signals were then multiplexed using two 3-dB optical couplers, and their power was equalized by adjusting the laser powers. The signals were amplified by an EDFA before being transmitted over 10 km SMF to the RAU. Due to the optical LO at the RAU, the three baseband channels were all heterodyned in the PD, which generated three RF signals with 3 GHz spacing in the V-band at 59 GHz, 62 GHz, and 65 GHz. Finally, these RF signals were amplified and radiated by the SIW LWA in three different directions. To evaluate the BERs, the receiver was then moved to the three corresponding user positions. In Figure 12, the measured BERs of the simultaneously transmitted signals are depicted. While a clear power penalty w.r.t single beam operation and a power penalty between the individual beams was observed, still all three beams could be detected simultaneously using FEC. The achieved cell capacity in this case was 3 Gbit/s. This performance could of course be further improved using OFDM waveforms and higher-order modulation formats such as QAM. Performance degradation occurs because, in contrast to a mixer, the SBD detector downconverts all incoming V-band signals to baseband. Thus, the signals incur interference to each other, which can be estimated based on the sidelobe suppression of the SIW LWA at the used frequencies. This creates an outlook for future antenna optimization for these use cases.

The proposed concept of RAUs using SIW LWAs can fulfill the key requirements for a 5G hot-spot, which is to support multiple mobile users with a high data rate downlink service in a small and densely populated cell. It furthermore supports a centralized radio access architecture with fiber-optic fronthaul, as beam steering functionality is remoted to the central unit. The chosen wireless receiver technology with a simple SBD furthermore enables fabrication of low-cost mobile units.

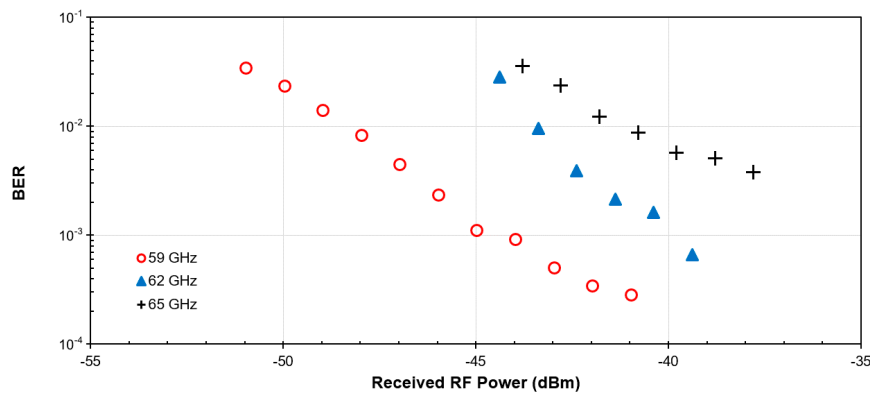


Figure 12. Measured BER over received RF power for three simultaneously transmit 1 Gbit/s OOK data signals at radio frequencies of 59 GHz (circles, red) 62 GHz (triangles, blue) and 65 GHz (crosses, black).

5. Conclusions

In this paper, a compact and low-cost SIW LWA for 60 GHz band operation, and it was used to support multiple users in a 60 GHz hot-spot.

PCB-based SIW LWAs providing 1D beam steering and multibeam operation in the V-band have been designed and fabricated. The antennas showed a peak gain of 15.4 dBi and over 40° beam steering in the H-plane. To overcome the well-known broadside problem of LWAs, arrayed microstrip radiating elements and unit cell asymmetry were applied to the antenna design. This way, a flat gain with a variation of ± 1.5 dB was achieved, even around broadside.

Furthermore, a novel approach for generating multiple steerable beams with the LWA is presented. By using DWDM and remote optical heterodyning, multiple RF carriers were generated at the feeding point of the LWA. Because of the different carrier frequencies of the RF signals, they were inherently radiated into different directions by the LWA. By changing the wavelength of an optical carrier, and thus the radio frequency fed to the LWA, the direction of the individual beam could be steered. By using multiple optical DWDM carriers, multiple steerable beams were generated simultaneously.

This approach was then used to support single and multiple users in a 60 GHz hot-spot. For a single user, a maximum data rate up to 2.5 Gbit/s was achieved using OOK modulation. For three users, each supported by an individual beam, a maximum cell capacity of 3 Gbit/s was experimentally demonstrated.

6. Patents

A German patent application titled “Funkzugangseinrichtung für ein Netzwerk mit faseroptischer Datenübertragung und entsprechendes Netzwerk” with the number 102017115638.0 has been filed by University of Duisburg-Essen, which concerns the presented SIW LWA and its described application for beam steering and multiuser support in a fiber-wireless communication system.

Acknowledgments: This work was supported in part by the Horizon2020 EU-JP research project RAPID5G (www.rapid-5g.eu or www.rapid-5g.jp) under the grant no. 643297.

Author Contributions: M.S. designed the antenna; N.Y. provided the antenna characterization and supported the data analysis; M.S., J.T., and A.S. conceived and designed the data transmission experiments; M.S. and J.T. performed the data transmission experiments; M.S. and A.S. analyzed the data; M.S. and A.S. wrote the paper.

Conflicts of Interest: The authors declare no conflict of interest. The founding sponsors had no role in the design of the study; in the collection, analyses, or interpretation of data; in the writing of the manuscript; or in the decision to publish the results.

References

1. Jiang, D.; Liu, G. An Overview of 5G Requirements. In *5G Mobile Communications*, 1st ed.; Xiang, W., Zheng, K., Shen, X., Eds.; Springer: Cham, Switzerland, 2016; pp. 3–26. ISBN 978-3-319-34208-5.
2. Rappaport, T.S.; Sun, S.; Mayzus, R.; Zhao, H.; Azar, Y.; Wang, K.; Wong, G.N.; Schulz, J.K.; Samimi, M.; Gutierrez, F. Millimeter Wave Mobile Communications for 5G Cellular: It Will Work! *IEEE Access* **2013**, *1*, 335–349. [[CrossRef](#)]
3. Weiler, R.J.; Peter, M.; Keusgen, W.; Calvanese-Strinati, E.; De Domenico, A.; Filippini, I.; Capone, A.; Siaud, I.; Ulmer-Moll, A.M.; Maltsev, A.; et al. Enabling 5G backhaul and access with millimeter-waves. In Proceedings of the 2014 European Conference Networks and Communications (EuCNC), Bologna, Italy, 23–26 June 2014. [[CrossRef](#)]
4. Chandra, K.; Venkatesha Prasad, R.; Niemegeers, I. An architectural framework for 5G indoor communications. In Proceedings of the 2015 International Wireless Communications and Mobile Computing Conference (IWCMC), Dubrovnik, Croatia, 24–28 August 2015. [[CrossRef](#)]
5. Cisco Visual Networking Index: Global Mobile Data Traffic Forecast Update, 2016–2021. Available online: <https://www.cisco.com/c/en/us/solutions/collateral/service-provider/visual-networking-index-vni/mobile-white-paper-c11-520862.html> (accessed on 14 October 2017).
6. Roh, W.; Seol, J.Y.; Park, J.; Lee, B.; Lee, J.; Kim, Y.; Cho, J.; Cheun, K.; Aryanfar, F. Millimeter-wave beamforming as an enabling technology for 5G cellular communications: Theoretical feasibility and prototype results. *IEEE Commun. Mag.* **2014**, *52*, 106–113. [[CrossRef](#)]
7. Marnat, L.; Dussopt, L.; Puyal, V.; Siligaris, A.; Hameau, F.; Larie, A.; Dehos, C. V-band transceiver modules with integrated antennas and phased arrays for mmWave access in 5G mobile networks. In Proceedings of the 2017 11th European Conference Antennas and Propagation (EUCAP), Paris, France, 19–24 March 2017. [[CrossRef](#)]
8. Lannoo, B.; Dixit, A.; Colle, D.; Bauwelinck, J.; Dhoedt, B.; Jooris, B.; Moerman, I.; Pickavet, M.; Rogier, H.; Simoons, P.; et al. Radio-over-fibre for ultra-small 5G cells. In Proceedings of the 2015 17th International Conference Transparent Optical Networks (ICTON), Budapest, Hungary, 5–9 July 2015. [[CrossRef](#)]
9. Cohen, E.; Ruberto, M.; Cohen, M.; Degani, O.; Ravid, S.; Ritter, D. A CMOS Bidirectional 32-Element Phased-Array Transceiver at 60 GHz with LTCC Antenna. *IEEE Trans. Microw. Theory Tech.* **2013**, *61*, 1359–1375. [[CrossRef](#)]
10. Zhu, J.; Peng, B.; Li, S. Cavity-backed high-gain switch beam antenna array for 60-GHz applications. *IET Microw. Antennas Propag.* **2017**, *11*, 1776–1781. [[CrossRef](#)]
11. Cicchetti, R.; Miozzi, E.; Testa, O. Wideband and UWB Antennas for Wireless Applications: A Comprehensive Review. *Int. J. Antennas Propag.* **2017**, 1–45. [[CrossRef](#)]
12. Hong, W. Solving the 5G Mobile Antenna Puzzle: Assessing Future Directions for the 5G Mobile Antenna Paradigm Shift. *IEEE Microw. Mag.* **2017**, *18*, 86–102. [[CrossRef](#)]
13. Oliner, A.A.; Jackson, D.R. Leaky-Wave Antennas. In *Antenna Engineering Handbook*, 4th ed.; Volakis, J.L., Ed.; McGraw-Hill: New York, NY, USA, 2007; Chapter 11; ISBN 978-0071475747.
14. Liu, J.; Jackson, D.R.; Long, Y. Substrate Integrated Waveguide (SIW) Leaky-Wave Antenna with Transverse Slots. *IEEE Trans. Antennas Propag.* **2012**, *60*, 20–29. [[CrossRef](#)]
15. Otto, S.; Caloz, C. Importance of transversal and longitudinal symmetry/asymmetry in the fundamental properties of periodic leaky-wave antennas. In Proceedings of the 2013 IEEE AP-S International Symposium (APSURSI), Orlando, FL, USA, 7–13 July 2013. [[CrossRef](#)]
16. Steeg, M.; Khani, B.; Rymanov, V.; Stöhr, A. Novel 50–70 GHz Compact PCB Leaky-Wave Antenna with High Broadside Efficiency and Low Return Loss. In Proceedings of the 41st International Conference Infrared, Millimeter and Terahertz Waves (IRMMW-THz), Copenhagen, Denmark, 25–30 September 2016. [[CrossRef](#)]
17. Bozzi, M.; Pasian, M.; Perregrini, L.; Wu, K. On the losses in substrate integrated waveguides. In Proceedings of the 2007 European Microwave Conference, Munich, Germany, 9–12 October 2007. [[CrossRef](#)]
18. Salehi, M.; Mehrshahi, E. A Closed-Form Formula for Dispersion Characteristics of Fundamental SIW Mode. *IEEE Microw. Compon. Lett.* **2011**, *21*, 4–6. [[CrossRef](#)]
19. Davidson, D.B. *Computational Electromagnetics for RF and Microwave Engineering*, 2nd ed.; Cambridge University Press: Cambridge, UK, 2010; ISBN 978-0521518918.

20. Southwest Microwave, Inc. The Design and Test of Broadband Launches up to 50 GHz on Thin and Thick Substrates. Available online: <http://mpd.southwestmicrowave.com/resources/> (accessed on 20 November 2017).
21. Lafond, O.; Himdi, M. Substrates characterisation (ϵ_r , $\tan \delta$) up to millimeter wavelength. In Proceedings of the 2004 10th International Symposium Antenna Technology and Applied Electromagnetics and URSI Conference (ANTEM), Ottawa, ON, Canada, 20–23 July 2004. [[CrossRef](#)]
22. Balanis, C.A. *Antenna Theory: Analysis and Design*, 4th ed.; John Wiley & Sons: Hoboken, NJ, USA, 2016; ISBN 978-1118642061.
23. Steeg, M.; Stöhr, A. High Data Rate 6 Gbit/s Steerable Multibeam 60 GHz Antennas for 5G Hot-Spot Use Cases. In Proceedings of the 2017 IEEE Photonics Society Summer Topical Meeting Series (SUM), San Juan, Puerto Rico, 10–12 July 2017. [[CrossRef](#)]



© 2017 by the authors. Licensee MDPI, Basel, Switzerland. This article is an open access article distributed under the terms and conditions of the Creative Commons Attribution (CC BY) license (<http://creativecommons.org/licenses/by/4.0/>).